

Towards automatic interpretation of sheep ultrasound scans

C.A. Glasbey
Scottish Agricultural Statistics Service
JCMB, King's Buildings, Edinburgh EH9 3JZ, Scotland

I. Abdalla
Department of Mathematics and Statistics, University of Edinburgh
JCMB, King's Buildings, Edinburgh EH9 3JZ, Scotland

and G. Simm
Genetics and Behavioural Sciences Department,
Scottish Agricultural College
West Mains Road, Edinburgh EH9 3JG, Scotland

Abstract – Ultrasound imaging is widely used in animal breeding to provide *in vivo* estimates of the carcass composition of candidates for selection. Although the technique is less accurate than more recent medical imaging methods, such as X-ray computed tomography and magnetic resonance imaging, it is relatively cheap and mobile. Therefore large numbers of animals can be measured. Most current ultrasound scanners require some degree of manual interpretation of images, which is time consuming and liable to vary both between and within individuals. Hence, this study investigated the automatic interpretation of ultrasound scans from sheep. A computer algorithm is proposed for identifying tissue boundaries. Estimates of tissue depth are shown to be comparable with those obtained by manual interpretation, for images of seventy two sheep scanned twice at the position of the 13th thoracic vertebra. The root-mean-square errors of subcutaneous fat depth and *m. longissimus* muscle depth were 0.7mm and 1.7mm, respectively.

Key words – Eye-muscle depth, Fat depth, Image analysis, Suffolk sheep.

1 Introduction

Non-invasive imaging techniques such as ultrasound, X-ray tomography (CT) and magnetic resonance imaging (MRI) are widely used in human medicine today. They also have great potential in animal science and production, because tissue boundaries can be mapped and used to predict body composition (Simm, 1983 and 1992). Ultrasound uses cheaper and more-mobile imaging equipment than either CT or MRI. Largely for these reasons, this technique has become widely used in animal breeding to assist in selection for leaner carcasses. However, ultrasound images are far more susceptible to noise than those from CT or MRI (see Fig 1 for a typical example). Therefore, most ultrasound images require some degree of manual interpretation. This is very time consuming, because experimental and industry selection programmes usually involve many animals, and variation between and within interpreters (and operators) may limit the precision of the technique. For a thorough examination of factors affecting the reproducibility of ultrasonic scanning, see Miles *et al* (1972) and other studies cited in the reviews of Alliston (1983) and Simm (1983).

Partly to circumvent problems of subjective assessment of images, ultrasound transmission techniques have been investigated (eg Miles *et al*, 1984). These produce direct estimates of body composition, based on the relationship between the reciprocal of the speed of transmission of ultrasound across the body, and the fat content of the tissue through which the sound has travelled. Whilst these techniques give broadly similar precision of prediction of composition to pulse-echo methods (Simm, 1987), the latter are more widely used to date. This is partly because measurements of tissue depths or areas have direct value in some cases. Hence, the interest in automatic methods for interpreting ultrasound pulse-echo scans.

Currently, in the Scottish Agricultural College, ultrasound scans are interpreted manually. A mouse is used to control a screen cursor and identify tissue boundaries, in order to measure average fat depth and maximum eye-muscle depth. In this paper, an algorithm is proposed for identifying tissue boundaries in thoracic ultrasound scans of sheep without any human intervention. It was developed using a subset of 20 images, and subsequently validated on a set of 144 images by making comparisons with results obtained by human interpretation.

We are unaware of other published work on automatic interpretation of sheep ultrasound scans. However, there are several papers on ultrasonic applications with humans. For example, Lin *et al* (1991) used a Bayesian approach to detect boundaries in abdominal images, whereas Baldock (1992) and Cootes *et al* (1994) proposed the use of trainable models for the interpretation of echocardiograms. For a broader discussion of the issues involved in using a computer to analyse images, see Glasbey

and Horgan (1995).

2 Materials and methods

A Vetscan MKI, real time, 'B' mode, ultrasonic scanner with a 56mm, 5MHz transducer was used in this experiment. It produces images which are typical of most modern pulse-echo machines. The animals scanned were 72 female Suffolk lambs. Their average liveweight was 60kg (s.d. 6kg), and they were part of an experiment to investigate selection for improved carcass composition in sheep (Simm *et al*, 1990). Each sheep was scanned twice, a week apart, such that the average age at scanning was 150 days of age, with a range of 4 days. The sheep were scanned at two locations, namely, the 13th thoracic vertebra (last rib) and the 3rd lumbar vertebra. There are few muscles at these locations and their anatomy is relatively simple, which aids interpretation of scans. At both these locations the transducer was positioned so the scan began at approximately the midline.

Pulse-echo ultrasound instruments operate by sending a pulse of sound waves of very high frequency into a subject. When the ultrasound wave meets a boundary between two tissues, partial reflection occurs. The greater the difference in acoustic impedance between the two tissues, the greater the reflection. For example, more energy is reflected from a muscle-bone interface than from a muscle-fat one. The reflected energy is received by the instrument and converted into electrical signals which are displayed on a video monitor, with time delay interpreted as depth. The topmost, approximately horizontal, light-grey band in Fig 1, which is a thoracic image, is the transducer-skin boundary. Below this are further light-grey bands corresponding to the skin-fat boundary, a boundary within the subcutaneous fat layer, and the fat-muscle boundary. The backbone appears as a light-grey area in the bottom left of the image, from which a rib can be seen sloping slightly upwards. The muscle above this bone is the *m. longissimus* or eye-muscle.

At the first scanning occasion, instrument settings such as overall- and near-gain, brightness and contrast, were adjusted to give the best visual contrast between tissues, and were then left in these positions, with only a few exceptions when images were difficult to obtain. The screen-displayed images used eight shades of grey. Each image was photographed using a Polaroid PCU-100 camera mounted in a black box at a fixed distance from the screen, and printed on black and white 8.5cm \times 10.8cm Polaroid (ISO 200/24⁰) film. Good reproduction of the original grey scale was achieved. The photographs produced were 1.24 \times the live animal scale. The central parts of the photographs were subsequently digitized to 401 \times 341 arrays with 256 grey-levels, at a resolution of 7.9 pixels/mm using a Hewlett Packard ScanJet

Plus desktop scanner. Combining these two conversions together, the scaling factor works out as 1 pixel corresponding to 0.157mm of tissue depth in the sheep. This indirect method of data transfer between computers was used because the Vetscan machine had no video output. It is both time consuming and a source of additional noise in the images, in particular producing the vertical display lines which can be discerned in Fig 1.

2.1 Algorithm

The algorithm for interpreting the digitized scans proceeds in three stages. First, the angle of orientation of the digitized photograph is identified. Misalignment of Polaroid prints in the scanner was only slight, but is critical to later stages in the algorithm and so has to be corrected. Secondly, horizontal boundaries are found corresponding to the top and bottom of the fat layers, using a method akin to a Hough transform (see for example, Leavers, 1992). Finally, the top of the rib is located. Details of the three stages follow, using the image in Fig 1 for illustration.

2.1.1 Image orientation

Let $X_{i,j}$ denote the image intensity at pixel location (i, j) , that is, the element in row i , column j . A large value of $X_{i,j}$ indicates a bright pixel, whereas a value near zero represents a dark area in the ultrasound image.

In order to identify the image orientation, the position of the transducer-skin boundary is determined on the left and right sides of the image, by finding the brightest row of pixels in the first and last 41 columns. The left and right ends of the boundary are estimated to be in rows i_l and i_r , defined as follows:

$$i_l = \operatorname{argmax}_{i=0\dots 200} \sum_{j=0}^{40} X_{i,j} \quad \text{and} \quad i_r = \operatorname{argmax}_{i=0\dots 200} \sum_{j=300}^{340} X_{i,j}.$$

Here ‘argmax’ denotes that i_l and i_r are set to the values of i which maximize the summations. The \times ’s on Fig 1 indicate the selected positions in rows 88 and 85 for this illustrative image. From these results, the slope of the image is calculated as:

$$s = \frac{i_r - i_l}{300}$$

In the case of Fig 1, the slope is -0.010 .

2.1.2 Fat layer

The top and bottom boundaries of the fat layer are assumed to be horizontal in the original photograph, and are therefore at slope s in the digitized image. The restriction to a horizontal boundary, which is only an approximation to the truth, is made for simplicity and in order for the algorithm to be robust. Boundaries are discontinuous in some ultrasound images and it is difficult even for the human eye to follow them.

As a first step in locating these horizontal boundaries, the summed image intensity along each sloping row of the image is derived as:

$$Y_i = \sum_{j=0}^{340} X_{[i+(j-170)s],j} \quad \text{for } i = 0, \dots, 400,$$

where $[\]$ denotes ‘rounding to the nearest integer’ and $X_{k,j}$ is set to 0 if k lies outside the range 0 to 400. Fig 2 shows the Y ’s obtained from Fig 1. Essentially, this is equivalent to an ‘A’ mode ultrasound scan, in which a one-dimensional signal is produced instead of an ultrasound image, though it has been obtained by other means.

From these row sums, the row index i_t corresponding to the top of the image is obtained as the value of i which maximizes Y_i , i.e.

$$i_t = \operatorname{argmax}_{i=0\dots400} Y_i.$$

In Fig 2, the maximum occurs at $i_t = 86$. The point is marked by the left-most \times .

The top of the fat layer is found as the first local maximum of Y_i which exceeds 20% of Y_{i_t} and is more than 10 rows below i_t . Therefore, i_f is found as the smallest value of i such that

$$i > i_t + 10 \quad , \quad Y_{i-1} \leq Y_i < Y_{i+1} \quad \text{and} \quad Y_i \geq \frac{1}{5} Y_{i_t}.$$

These constraints ensure that the skin layer is at least 10 pixels thick, and that fluctuations in low values of Y in the skin layer, produced by noise, are not misinterpreted as being a real boundary. These particular limits were chosen after carefully examining the 20 original images. For Fig 2, the maximum is identified as $i_f = 115$, and is marked by the central \times . The corresponding boundary is shown in Fig 1 as the topmost dotted line superimposed on the image. A valid value of i was found in all our applications of this rule. If, in future, exceptions are encountered, we suggest that i_f is set to its mean value of $(i_t + 28)$.

Similarly, the top of the muscle layer is found as the last local maximum of Y_i which exceeds 60% of Y_{i_f} and is less than 100 rows below i_t . Therefore, i_m is found as the largest value of i such that

$$i_f \leq i < i_t + 100 \quad , \quad Y_{i-1} \leq Y_i < Y_{i+1} \quad \text{and} \quad Y_i \geq \frac{3}{5}Y_{i_f}.$$

The combined skin and fat depths are thereby constrained to be less than 100 pixels. A value of i can always be found, because $i = i_f$ satisfies the constraints. For Fig 2, the rule that $i_m < i_t + 100$ excludes the maximum when $i = 310$, and the rule that $Y_{i_m} \geq \frac{3}{5}Y_{i_f}$ excludes the maximum at $i = 185$. The top of the eye-muscle is found to be on row 143, which is marked by the right-most \times in Fig 2. The boundary is shown by the second-from-top dotted line in Fig 1.

2.1.3 Rib

We have to adopt a slightly more complicated approach to locate the rib, because it is not horizontal or straight, nor does it cross the whole image. Therefore, we chose to specify it as a parabola excluding the left-most quarter of the image. (Strictly speaking, in referring to the bone in what follows, we actually mean the two-dimensional intersection of the rib with the plane of the image.) A parabola requires three parameters to specify it: we use i to locate the maximum depth of the bone, which we assume to occur in column 85, α to specify the angle of the slope of the the bone at this point, and β to control the curvature of the parabola. The row-location of the parabola in column j is given by $i - g(\alpha, \beta, j)$ where

$$g(\alpha, \beta, j) = (j - 85) \tan \alpha - (j - 85)^2 \frac{\beta}{10000}.$$

(The divisor of 10000 is to allow β to take integer values.) In the same way that the earlier boundaries were located as the brightest horizontal lines in restricted positions in an ultrasound image, so the rib is located as the section of a parabola in the bottom part of the image which has the greatest summed pixel intensity. Values are obtained as:

$$(i_b, \alpha_b, \beta_b) = \operatorname{argmax}_{(i, \alpha, \beta) \in C} \sum_{j=85}^{340} X_{[i-g(\alpha, \beta, j)], j} \quad ,$$

where C is the set of triples (i, α, β) over the ranges:

$$i = (i_m + 170), \dots, 400 \quad , \quad \alpha = 0, \dots, 50 \quad , \quad \beta = 0, \dots, 20 \quad ,$$

subject to the restrictions that the right end of the parabola is no lower than the left end, and is at least 40 rows below i_m , i.e.

$$g(\alpha, \beta, 255) \leq 0 \quad \text{and} \quad [i - g(\alpha, \beta, j)] \geq i_m + 40.$$

For Fig 1, the maximum occurs when $(i_b, \alpha_b, \beta_b) = 397, 32, 10$, which specifies the curved boundary shown as the dotted curve at the bottom of Fig 1. Use of a parametric curve for the rib seems adequate in this application. An alternative approach, which could also incorporate information about the backbone, would be to construct a grey-scale template and match it to each ultrasound scan (Amit, Grenander and Piccioni, 1991). For example, another imaging modality, such as CT, could be used to provide a template (Moshfeghi, 1991, Abdalla, 1994).

3 Results

The algorithm was applied to the 2 thoracic images, obtained one week apart for each of the 72 sheep. As already discussed, the results for one image are shown in Fig 1. For comparison, the figure also shows as continuous white lines the manually-obtained boundaries for the same image. Various aspects of the algorithm, such as the limits applied in the derivations of i_f and i_m , were chosen after careful examination of 20 images. The remaining 124 images therefore provide a validation of the method, albeit with the caveat that they were images from the same experiment.

Fig 3(a) shows the estimated fat depths on week one for all 72 sheep, with the manual results plotted against the output from the algorithm, i.e. $(i_m - i_f)$. The agreement is good, although it can be seen that the automatic method appears to underestimate the fat depth. This is because boundaries are positioned to maximize image intensity, whereas the hand-drawn lines are placed further apart. The bias can be corrected for, by regressing the manual results on the automatic ones, which gives an unbiased estimator of fat depth of

$$19 + 0.89(i_m - i_f).$$

The regression line is shown in Fig 3(a). The intercept term, 19, adjusts for the apparent underestimation in the automatic method. The residual standard deviation, or equivalently the root-mean-square error, is 4.6, which converts to 0.7mm. For comparison, the average fat depth is 42 pixels, or 6.6mm.

Fig 3(b) shows manually estimated fat depths for weeks one and two plotted against each other. The average fat depth increased to 45 pixels on the second scan occasion. The root-mean-square difference in results is 5.0, after allowing for this change in mean value of 3 pixels (0.5mm). Therefore, there appears to be no greater consistency in results between the two hand-drawn interpretations than with output from the algorithm. This is borne out in Table 1, which shows all root-mean-square differences between manual and automatic estimates of fat depth on the two scan

dates. The calibration equation derived for the automatic method in week one was applied to the data in week two without any re-estimation.

Eye-muscle depth estimates were calibrated between the automatic and manual methods, by regressing the manual results for the scans on week one against $(i_b - i_m)$, α_b and β_b from the automatic algorithm. The coefficient in β_b was not significantly different from zero, so the predictor of muscle depth was simplified to

$$51 + 0.77(i_b - i_m) - 0.68\alpha_b.$$

Note that the manual method for measuring eye-muscle depth is best predicted by the maximum depth from the automatic algorithm only after an adjustment has been made for the slope of the rib (α_b). The root-mean-square error is 10.6 pixels, which converts to 1.7mm for an average eye-muscle depth of 32.4mm. If the α_b term is omitted from the predictor, then the root-mean-square error is 1.9mm. Fig 3(c) is a plot of muscle depths on the first scan occasion: the manually-obtained result is plotted against that derived from the algorithm. Agreement can be seen to be better than that in Fig 3(d), which shows manual results from weeks one and two plotted against each other. Comparisons between methods and weeks, shown in Table 2, confirm that the algorithm estimates eye-muscle depth at least as accurately as the manual method.

4 Discussion

Ultrasound imaging has become a widely used tool in animal production over the past few decades. Although more advanced imaging techniques such as CT and MRI may give more precise prediction of body composition, their high cost and relative immobility severely limit their application in agriculture. Even when these techniques are available, they are likely to be used only for ‘second-stage’ selection of a relatively small number of animals, pre-selected from a much wider population using ultrasound measurements. The utility of ultrasound imaging would be further increased if it could be made easier, quicker or cheaper to use, or if the precision of results were improved. At present, measurements are obtained from ultrasound images either by recording the image in some way, followed by later interpretation (as in the example used here), or by temporarily freezing an image on the screen of the imaging machine to allow interpretation at the time of imaging. Automation of interpretation offers potential advantages in both these cases. In the former case it can reduce the tedious and time consuming tasks involved in obtaining detailed measurements from recorded images. In the latter case it could, in future generations of imaging machines, allow more repeatable and comprehensive measurements

to be obtained from images under field conditions, where speed of operation and rapid availability of results are important.

The algorithm proposed here is simple but effective. In some of the scans most severely contaminated with noise, boundaries were slightly misplaced, as shown by a few outlying points in Fig 3(a). However, the level of uncertainty remained no higher than that obtained with hand-drawn boundaries. (If contamination by noise was more severe, a filter such as that proposed by Loupas *et al* (1989) could be used.) Various subjectively-chosen constraints in the algorithm will probably need modification for use with other sheep breeds, scanning positions or types of scanner. Also, the representation of the top of the eye-muscle by a horizontal line is only an approximation to the true, curved boundary. This is particularly true for images obtained at the alternative scanning location, the 3rd lumbar vertebra. However, an approach similar to that used for locating the rib could be adopted.

Acknowledgements

We are grateful to Sue Murphy for scanning the sheep and interpreting the scans. This work was supported by funding from the Scottish Office Agriculture and Fisheries Department, and by the University of Khartoum, Sudan.

References

- Abdalla, I.** 1994. *Statistical Image Analysis of Sheep Ultrasound Scans*, M. Phil. Thesis, University of Edinburgh.
- Alliston, J.C.** 1983. Evaluation of carcass quality in the live animal. In *Sheep Production* (ed. H Haresign). Butterworth, London. pp. 75-95.
- Amit, Y., Grenander, U. and Piccioni, M.** 1991. Structural image restoration through deformable templates. *Journal of the American Statistical Association* **86**:376-387.
- Baldock, R.A.** 1992. Trainable models for the interpretation of biomedical images. *Image and Vision Computing* **10**:444-450.
- Cootes, T.F., Hill, A., Taylor, C.J. and Haslam, J.** 1994. Use of active shape models for locating structure in medical images. *Image and Vision Computing*

12:355-365.

Glasbey, C.A. and Horgan, G.W. 1995. *Image Analysis for the Biological Sciences*, Wiley, Chichester.

Leavers, V.F. 1992. *Shape Detection in Computer Vision using the Hough Transform*, Springer-Verlag, London.

Lin, W.J., Pizer, S.M. and Johnson, V.E. 1991. Boundary estimation in ultrasound images. In *Information Processing in Medical Imaging. Proceedings of the 12th International Conference on Information Processing in Medical Imaging* (ed. A.C.F. Colchester and D.J. Hawkes). Springer-Verlag, Berlin. pp. 285-299.

Loupas, T., McDicken, W.N. and Allan, P.L. 1989. An adaptive weighted median filter for speckle suppression in medical ultrasonic images. *IEEE Transactions on Circuits and Systems* **36**:129-135.

Moshfeghi, M. 1991. Elastic matching of multimodality medical images, *Computer Vision, Graphics and Image Processing* **53**:271-282.

Miles, C.A., Pomeroy, R.W. and Harries, J.M. 1972. Some factors affecting reproducibility in ultrasonic scanning of animals. 1. cattle. *Animal Production* **15**:239-249.

Miles, C.A., Fursey, G.A.J. and York, R.W.R. 1984. New equipment for measuring the speed of ultrasound and its application in the estimation of body composition of farm livestock. In *In Vivo Measurement of Body Composition in Meat Animals* (ed. D Lister). Elsevier, London. pp. 93-105.

Simm, G. 1983. The use of ultrasound to predict the carcass composition of live cattle – a review. *Animal Breeding Abstracts* **51**: 853-875.

Simm, G. 1987. Carcass evaluation in sheep breeding programmes. In *New Techniques in Sheep Production* (ed. IFM Maria and JB Owen). Butterworth, London. pp. 125-144.

Simm, G. 1992. Selection for lean meat production in sheep. In ‘*Recent Advances in Sheep and Goat Research*’, (ed A.W. Speedy). CAB International, pp 193-215.

Simm, G., Dingwall, W.S., Murphy, S.V. and FitzSimons, J. 1990. Selection for improved carcass composition in Suffolk sheep. *Proc. of 4th World Congress on Genetics Applied to Livestock Production* **XV**: 100-103.

Table 1: Root-mean-square differences between estimates of fat depth, expressed in pixel units (1 pixel represents 1.57mm of tissue).

	manual, week 1	manual, week 2	automatic, week 1	automatic, week 2
manual, week 1	–			
manual, week 2	5.0	–		
automatic, week 1	†4.6	6.0	–	
automatic, week 2	4.3	4.6	4.3	–

† value deflated through estimation of regression coefficients

Table 2: Root-mean-square differences between estimates of eye-muscle depth, expressed in pixel units (1 pixel represents 1.57mm of tissue).

	manual, week 1	manual, week 2	automatic, week 1	automatic, week 2
manual, week 1	–			
manual, week 2	14.6	–		
automatic, week 1	†10.6	12.4	–	
automatic, week 2	15.2	9.7	11.1	–

† value deflated through estimation of regression coefficients

Captions for figures

- Fig 1** Ultrasound image of a sheep, at the location of the 13th thoracic vertebra. Positions of the top of the skin layer on the left and right sides of the image are shown by \times 's. Also shown are tissue boundaries identified by the automatic algorithm, corresponding to the top and bottom of the fat layer and to the rib (\cdots), and the manually-identified top and bottom of the fat layer, and a line indicating maximum eye-muscle depth ($—$).
- Fig 2** Sum of intensities along each (sloping) row in Fig 1, plotted against row number. The three \times 's, from left to right, are the estimated locations of the transducer (i_t), the top of the fat layer (i_f) and the top of the muscle layer (i_m).
- Fig 3** Estimated fat and muscle depths for 72 sheeps: **(a)** manual estimate of fat depth on week one plotted against automatic estimate on week one, together with 1:1 line ($—$) and regression line ($- - -$); **(b)** manual estimate of fat depth on week one plotted against manual estimate on week two, together with 1:1 line ($—$); **(c)** manual estimate of muscle depth on week one plotted against automatic estimate on week one, together with 1:1 line ($—$); **(d)** manual estimate of muscle depth on week one plotted against manual estimate on week two, together with 1:1 line ($—$). Scales are expressed in pixel units (1 pixel represents 1.57mm of tissue).

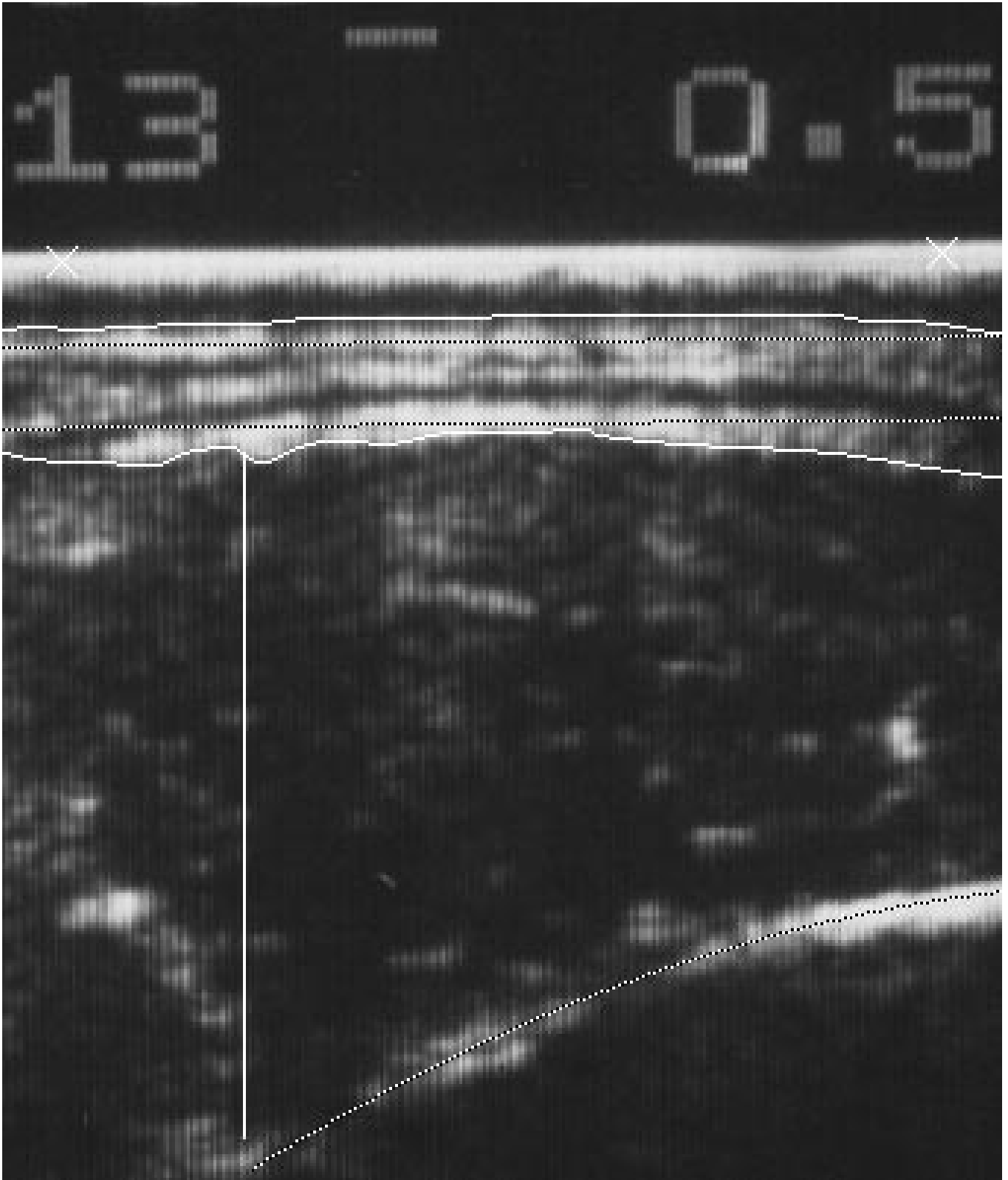


Fig 1

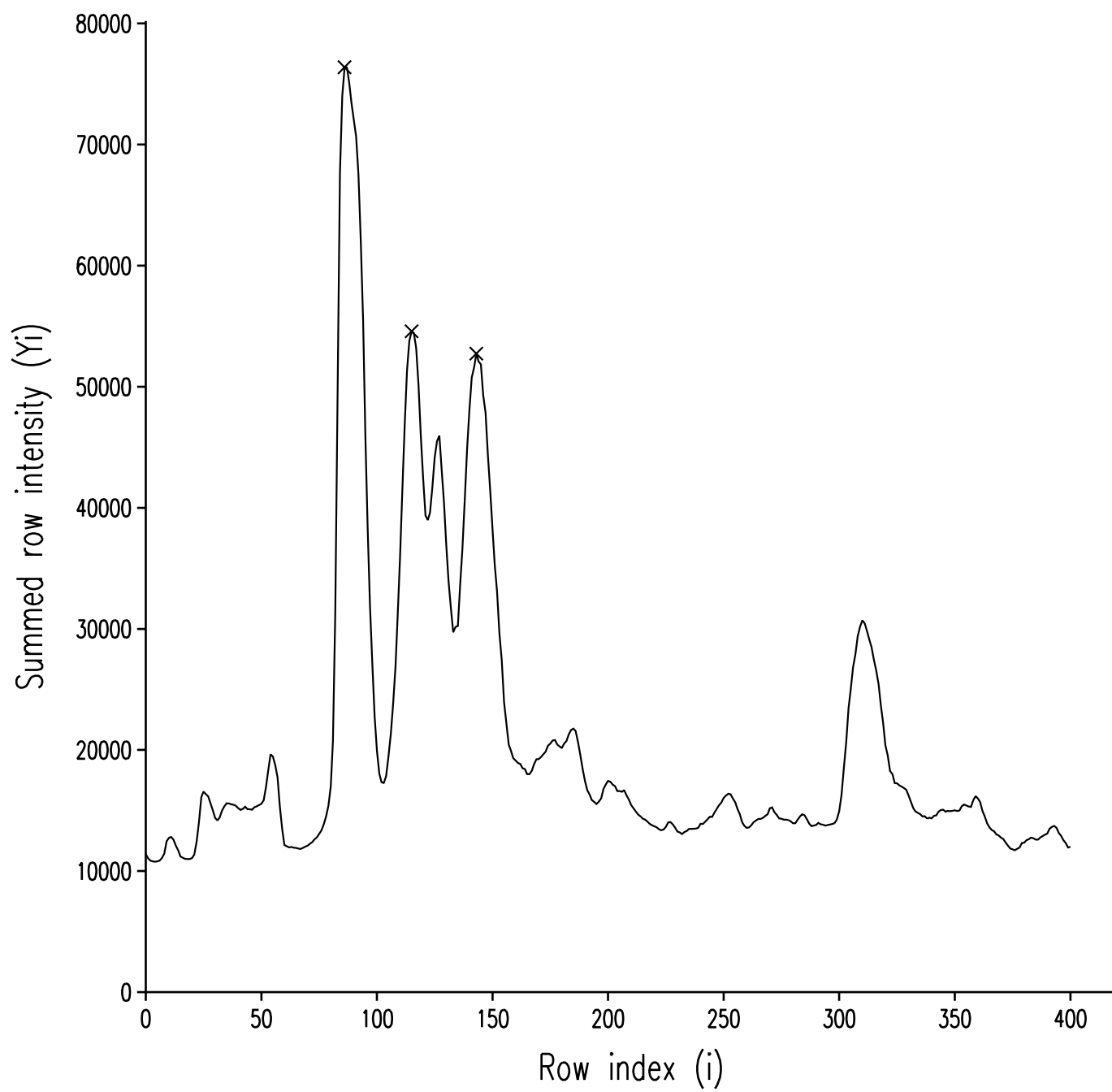


Fig 2

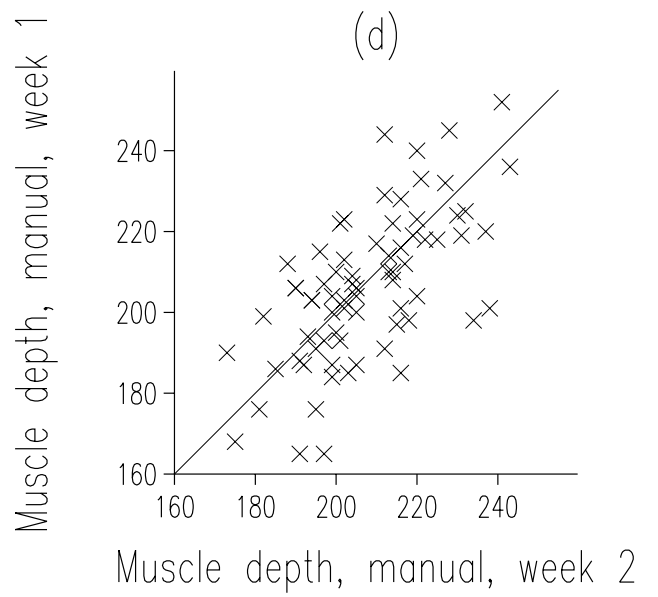
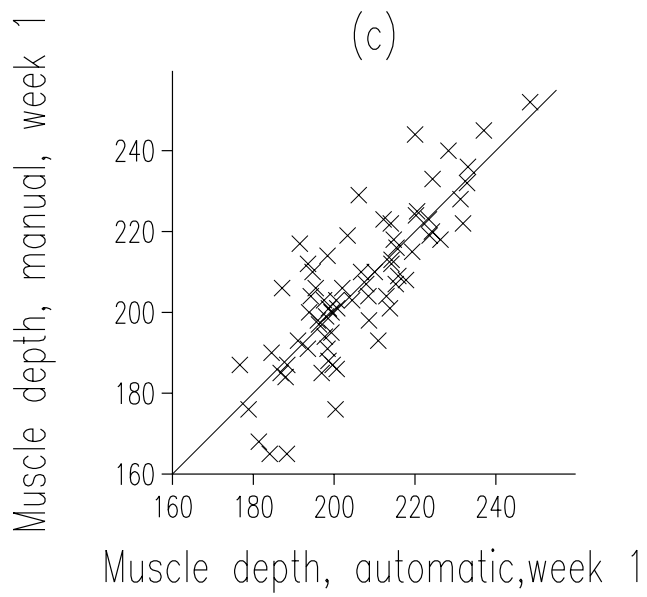
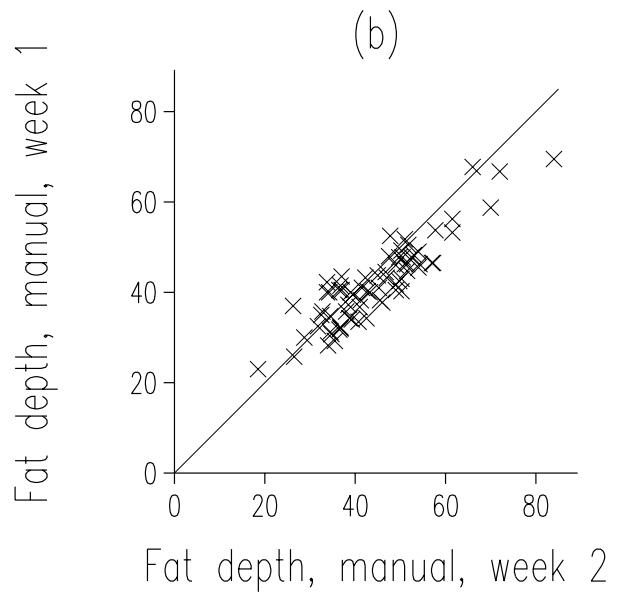
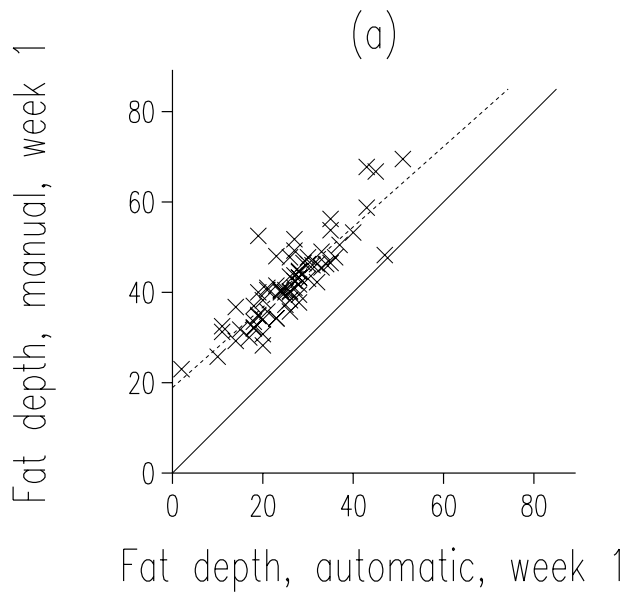


Fig 3